Recurrent frontal slicks of a coastal ocean upwelling shadow

J. P. Ryan,[1] A. M. Fischer,[1,2] R. M. Kudela,[3] M. A. McManus,[4] J. S. Myers,[5] J. D. Paduan,[6] C. M. Ruhsam,[3] C. B. Woodson,[7] and Y. Zhang[1]

Received 12 May 2010; revised 24 September 2010; accepted 6 October 2010; published 29 December 2010.

[1] Marine ecosystems are greatly influenced by the structure and dynamics of fronts. In coastal upwelling systems, frontogenesis occurs frequently by upwelling and transport of cold water and warming in sheltered "upwelling shadow" retention sites. Monterey Bay, in the California Current upwelling system, hosts a dynamic upwelling shadow environment. Using a decade of satellite synthetic aperture radar (SAR) observations with ancillary remote sensing and in situ data, we describe recurrent surface slicks that develop along the seaward periphery of the Monterey Bay upwelling shadow, and we examine their relationships with fronts. Slick median dimensions, 17.5 km long and 0.8 km wide, describe their elongated structure. Although the typical pattern is a single slick, multiple slicks may concurrently develop in association with different types of fronts. Repeated volume surveys through a front, underlying a slick, revealed lateral mixing and interleaving of regional water types. Velocity fields from coastal HF radar show that slicks may coincide with a variety of surface circulation patterns, that they may extend contiguously across regions having very different surface velocity, and that they may be separated from the shear front of upwelling filaments by 5–10 km. Slicks occur in all seasons and may coincide with both upwelling and downwelling wind forcing. Surfactant accumulation in small-scale convergence zones is indicated as the primary mechanism of slick formation, not ocean current shear or small-scale air-sea coupling. The results of this study emphasize the role of upwelling system fronts in creating small-scale structure and dynamics that influence plankton ecology.

Citation: Ryan, J. P., A. M. Fischer, R. M. Kudela, M. A. McManus, J. S. Myers, J. D. Paduan, C. M. Ruhsam, C. B. Woodson, and Y. Zhang (2010), Recurrent frontal slicks of a coastal ocean upwelling shadow, *J. Geophys. Res.*, *115*, C12070, doi:10.1029/2010JC006398.

1. Introduction

[2] Oceanic fronts exist across a vast range of spatial and temporal scales [*Belkin et al.*, 2009], and they shape the ecology of marine life across a great range of habitat and life-form scales. At the core of the food web, phytoplankton ecology is influenced by fronts in a variety of ways, including enrichment of growth conditions [*Pingree et al.*, 1975; *Simpson and Pingree*, 1978; *Yoder et al.*, 1981; *Pitcher et al.*, 1998; *Ryan et al.*, 1999a, 1999b, 2001, 2010a; *Moore and Abbott*, 2002; *Smayda*, 2002], aggregation and transport of biomass [*Ryan and Yoder*, 1996; *Tester and Steidinger*, 1997; *Anderson et al.*, 2005; *Ryan et al.*, 2005a, 2008a, 2009, 2010a; *Janowitz and Kamykowski*, 2006; *Skaröhamar et al.*, 2007; *Carreto et al.*, 2008], formation of thin biological layers by vertical shear [*Franks*, 1995; *Ryan et al.*, 2008b], and coupling of the mixed layer with the bottom boundary layer [*Ryan et al.*, 2005b]. Aggregation of biogenic surfactants at fronts has also been linked to a recently discovered mechanism by which dinoflagellate blooms can harm marine life [*Jessup et al.*, 2009]. In addition to supporting enriched phytoplankton populations as food resources for zooplankton, fronts may influence zooplankton ecology through population aggregation as well as transport patterns that determine the scales and geography of larval dispersal and recruitment [*Roughgarden et al.*, 1991; *Graham et al.*, 1992; *Uye et al.*, 1992; *McLaren et al.*, 1998; *Russell et al.*, 1999; *Acha and Macchi*, 2000; *Govoni et al.*, 2000; *Shanks et al.*, 2000; *Lough and Manning*, 2001; *Morgan et al.*, 2005; *Schiariti et al.*, 2006; *Sabates et al.*, 2007; *Skaröhamar et al.*, 2007; *Tilburg et al.*, 2009; *Woodson et al.*, 2007, 2009]. At higher trophic levels, the ecological significance of fronts is evident

[1]Monterey Bay Aquarium Research Institute, Moss Landing, California, USA.
[2]National Centre for Marine Conservation and Resource Sustainability, University of Tasmania, Launceston, Tasmania, Australia.
[3]Ocean Sciences Department, University of California, Santa Cruz, California, USA.
[4]Department of Oceanography, University of Hawaii at Manoa, Honolulu, Hawaii, USA.
[5]University Affiliated Research Center, University of California, Santa Cruz, Moffett Field, California, USA.
[6]Department of Oceanography, Naval Postgraduate School, Monterey, California, USA.
[7]Environmental Fluid Mechanics Laboratory, Department of Civil and Environmental Engineering, Stanford University, Stanford, California, USA.

0148-0227/10/2010JC006398

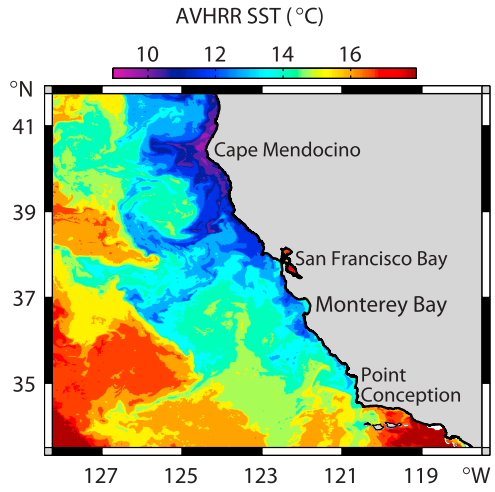

Figure 1. Sea surface temperature from the Advanced Very High Resolution Radiometer satellite sensor, 22 October 2008, 0537 UTC.

in the aggregation of foraging seabirds and marine mammals [*Haney and McGillivary*, 1985a, 1985b; *DiGiacomo et al.*, 2002; *Polovina et al.*, 2004; *Woehler et al.*, 2006; *Bost et al.*, 2009].

[3] Fronts abound in eastern boundary current systems, where wind-driven upwelling generates cold filaments that flow sinuously through ocean margin waters [e.g., *Flament et al.*, 1985; *Castelao et al.*, 2006]. Monterey Bay, California lies in the eastern boundary current system of the North Pacific (Figure 1), the California Current System (CCS). In the central CCS upwelling exhibits strong seasonal variation with peak upwelling during summer [*Bakun*, 1973; *Breaker and Broenkow*, 1994; *Pennington and Chavez*, 2000]. Sheltering from physical perturbation occurs in northern Monterey Bay due to its oceanographic recess in the lee of the Point Año Nuevo upwelling center, as well as its meteorological recess south of the Santa Cruz Mountains that reduce leeward exposure to strong northwesterly wind forcing [*Breaker and Broenkow*, 1994; *Rosenfeld et al.*, 1994]. This sheltering and its resultant ocean circulation patterns enhance residence time in the northern bay [*Graham and Largier*, 1997]. These effects of coastal geomorphology and their interactions with atmospheric and oceanic circulation are largely responsible for the phenomenon known as the Monterey Bay "upwelling shadow," hereafter MBUS. Early studies describing the MBUS examined its physical and biological distinction from adjacent cold, upwelled waters that flow into the bay [*Graham et al.*, 1992; *Graham*, 1993]. Subsequent studies have shown how the MBUS responds strongly to variations in wind forcing, from synoptic to seasonal time scales [*Rosenfeld et al.*, 1994; *Graham and Largier*, 1997; *Ramp et al.*, 2005, 2009; *Woodson et al.*, 2007, 2009], and how phytoplankton ecology is strongly modulated by this environmental variability [*Ryan et al.*, 2008b, 2009, 2010a].

[4] The offshore periphery of the MBUS is a key ecological boundary. Phytoplankton populations thrive on episodic nutrient supply within the warm MBUS, and different types of phytoplankton blooms incubate within and spread from there [*Ryan et al.*, 2005a, 2008a, 2008b, 2009, 2010a; *Kudela et al.*, 2008; *McManus et al.*, 2008; *Rienecker et al.*, 2008]. The MBUS seaward boundary typically coincides with an abrupt change in water temperature and color, increased zooplankton biomass and activity at higher trophic levels, surface slicks, and accumulation of buoyant macroalgae and foam that can mark convergence zones [*Graham et al.*, 1992; *Graham and Largier*, 1997; *Woodson et al.*, 2007]. The formation of slicks in convergent fronts, where surface roughness is damped by the accumulation of biogenic surfactants, is observed in many ocean margin environments [*Pingree et al.*, 1974; *Marmorino et al.*, 2002; *Belkin*, 2002]. Foraging seabirds may use visual slick detection to find and utilize biologically rich feeding areas [*DiGiacomo et al.*, 2002]. Because convergent frontal zones are dynamically and ecologically enhanced, methods of slick detection are valuable for ecological studies. The small scales on which frontal structure and dynamics occur challenge our ability to adequately observe them, and high-resolution observation is essential.

[5] Providing synoptic high-resolution imaging of ocean surface roughness, synthetic aperture radar (SAR) remote sensing is an effective method of detecting slicks, internal waves and other ocean physical phenomena [*Apel*, 2004; *Holt*, 2004; *Lyzenga et al.*, 2004]. Phytoplankton ecology studies in Monterey Bay have shown that SAR can indicate areas where physical-biological couplings occur, including influences of internal waves (IWs) on plankton ecology and development of slicks in biologically enriched frontal zones [*Ryan et al.*, 2005a, 2008a]. These earlier studies motivated this examination of a larger archive of SAR imagery. Utilizing a decade of satellite RADARSAT-1 SAR observations of Monterey Bay, this study examines recurrent patterns of slicks. Integrating the SAR image archive with multiplatform, multidisciplinary remote sensing and in situ data, we examine oceanographic processes underlying slicks.

2. Data and Methods

2.1. Remote Sensing

2.1.1. Satellite Synthetic Aperture Radar Remote Sensing

[6] This study utilized the archive of RADARSAT-1 (R1) satellite SAR imagery that is available through the Alaska Satellite Facility (ASF). The full archive was subset using the ASF data interface (http://ursa.asfdaac.alaska.edu), which supports query based on region of interest. The image boundaries returned from the query were examined in Google Earth to eliminate images certain to provide no coverage of Monterey Bay. Because copyright regulations preclude online provision of R1 preview images, image screening was conducted following local generation of preview images from the Level 1.5 data using the ASF MapReady software. Images from all R1 beam modes, ranging in spatial resolution from 12.5 m to 100 m, were examined. Primary screening involved elimination of images that (1) provided no coverage of the MBUS or (2) were redundantly acquired in rapid succession when the satellite passed over the bay. From primary screening, the 1,979 images acquired from ASF were reduced to 229 images that provided nonredundant coverage of the MBUS. All images that passed primary screening were processed with MapReady to amplitude images with a UTM projection and 50 m pixel size, and

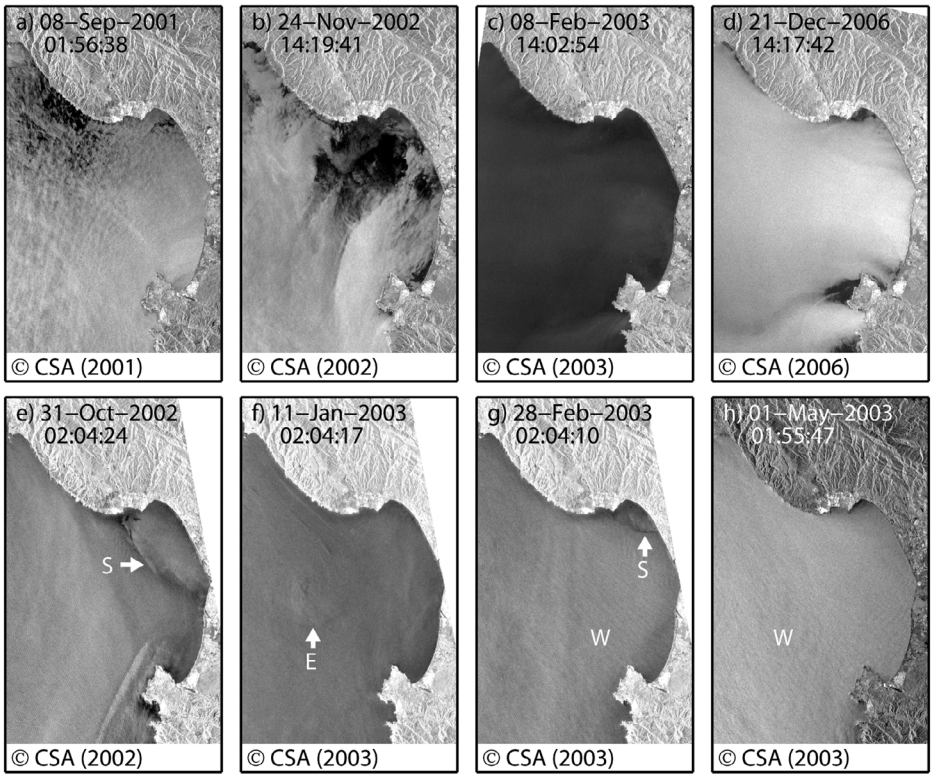

Figure 2. Illustration of the second stage of screening synthetic aperture radar images of the study region (section 2.1.1). (a–d) SAR images which were not included in the analysis of oceanographic patterns because of the apparent dominance of atmospheric signals. (e–h) SAR images which were included in the analysis of oceanographic patterns. Image acquisition times and dates are in UTC. Labels in Figures 2e–2h identify features described in the text (S, slick; E, eddy; W, wind rows).

secondary screening was applied based on image quality. Shown in Figures 2a–2d are characteristic examples of images that were excluded during secondary screening. These appeared to be dominated by atmospheric signals that occupied the low, high, or mixed low/high extremes of the dynamic range. Shown in Figures 2e–2h are characteristic examples of the 139 images that were retained for analysis. These appeared to be dominated by oceanic signals that occupied the mid- to low region of the dynamic range. In SAR images representing ocean surface roughness, dark areas indicate a relatively smooth sea surface, and bright areas indicate a relatively rough sea surface. Oceanographic features evident in the SAR images included elongated slicks (Figures 2e and 2g), eddies (Figure 2f), wind rows aligned with northwesterly upwelling winds outside the bay (Figures 2g and 2h), and packets of alternating light and dark banding within and outside the bay (Figures 2e, 2g, and 2h). This study focuses only on the elongated slicks (Figures 2e and 2g), which represent the most frequently detected pattern (n = 78, 56% of analysis images).

[7] Most of the images retained for analysis were acquired between 2002 and 2006 (Figure 3). All occurrences of slicks were identified for subsequent analysis of spatial scales and intensity, and coregistered SAR images of sigma data in dB were produced to quantify trough intensity. UTM coordinates tracing each slick's major axis were acquired using the MATLAB ginput function, and slick lengths were computed by summing the cumulative distance along the trace. Slick widths were computed from cross-slick profiles oriented perpendicular to the local major axis of the slick. Each dB

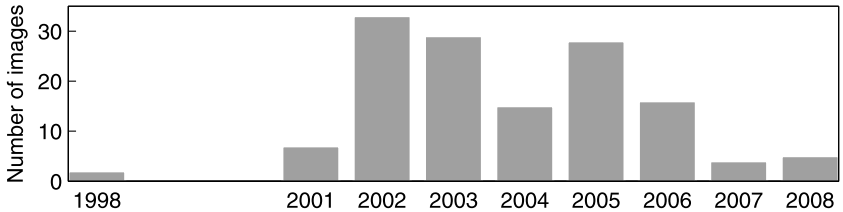

Figure 3. Histogram of the yearly counts for SAR images examined in this study.

profile extracted from the image was plotted versus distance in MATLAB, and the ginput function was used to acquire the distances, to each side of the trough minimum, at which the sigma gradient of the trough walls leveled off (the shoulders). Trough intensity was quantified as the depth of the trough below the linear baseline between the shoulders, and slick width was measured at the dB level of half of the trough minimum. For long slicks that exhibited variation in width and intensity, representative profiles were extracted and analyzed to sample this variation.

2.1.2. Satellite Infrared Remote Sensing

[8] This study used infrared data from the Advanced Very High Resolution Radiometer (AVHRR), 2004–2008. The AVHRR sensor constellation provides the greatest temporal resolution of high spatial resolution (1 km, Figure 1) coastal sea surface temperature (SST) data. This superior temporal resolution provides the best sampling for computing climatological means and optimizing the potential for near-concurrent matchup with SAR. Day and night SST images were acquired from the NOAA CoastWatch program, and the CoastWatch software for cloud removal [*Hollemans*, 2005] was applied. For each image, three different parameterizations of cloud masking were applied, each producing an image. Following this automated processing, manual processing was conducted using custom software developed for use in MATLAB. First, each set of three cloud-masked images was examined relative to the original image to select the one in which cloud masking was most effective. Second, the data content of the selected image was adjusted by either removing cloud contaminated pixels that were erroneously retained by the automated processing, or restoring ocean SST data that were erroneously removed by the automated processing. The seasonal SST climatology was computed from cloud-masked images for all years. We applied a standard definition of seasons as 3 month periods, beginning with spring as February–April [*Pennington and Chavez*, 2000]. To identify matching SST images for examination with SAR detection of slicks, we required the SST image acquisition time to be within 24 h of the SAR image acquisition time. We identified 15 SAR/SST image pairs having acquisition time differences of less than 24 h, and the four examples having the most complete SST coverage of the bay are examined in section 3.

2.1.3. Coastal HF Radar Remote Sensing

[9] A network of shore-based HF radar sites has been established around Monterey Bay for the purpose of mapping ocean surface currents. These instruments use Doppler radio wave backscatter in the frequency range between 12 and 25 MHz to infer the speed of the surface waters moving toward or away from the radar site; combination of input from two or more radar sites allows the mapping of vector surface currents with horizontal and temporal resolution around 3 km and 1 h, respectively, out to ranges of ~50 km [*Paduan and Graber*, 1997]. For the data used in this study, continuous surface current maps were available from 4 separate coastal HF radar sites. The instruments were the CODAR SeaSonde-type HF radar systems, which rely on direction-finding techniques to determine bearing information for the backscattered ocean signals [*Paduan and Graber*, 1997]. The remotely sensed velocity data respond directly to currents in the upper 1 m, although previous studies have shown that the vertical scale extends several tens of meters below the surface for subtidal period velocity fluctuations [e.g., *Paduan and Rosenfeld*, 1996]. Errors in the HF radar-derived velocities are variable, although extensive comparisons against in situ observations and radar-to-radar baseline observations in Monterey Bay during this study point to uncertainty levels around 12 cm s^{-1} for the hourly velocity maps [*Paduan et al.*, 2006]. To examine subtidal ocean surface circulation coincident with SAR, hourly HF radar current fields were averaged for 25 h period ending during the hour of SAR image acquisition. This averaging reduces uncertainty by ~35% (to ~8 cm s^{-1}). All possible matchups of SAR detection of a slick and surface currents were examined, and representative examples having full HF radar coverage of the bay are presented.

2.2. In Situ Sensing

2.2.1. Autonomous Underwater Vehicle Surveys

[10] We used a database of autonomous underwater vehicle (AUV) surveys in the Monterey Bay region to examine in situ conditions coincident with SAR observations of surface slicks. All survey data were acquired with the *Dorado* AUV executing along-track yoyo vertical profiling between ~2 m depth and ~5 m above bottom. The acquisition and processing of AUV hydrographic and optical data have been documented [*Ryan et al.*, 2008a]. To examine near-surface currents for two cases in which the AUV traversed frontal zones beneath slicks, we used current velocity measurements acquired with a down-looking Teledyne RDI 300 kHz Workhorse Navigator Doppler Velocity Log (DVL). The DVL measures current velocity relative to the AUV in an underlying 10 m layer. Because the seabed was within range during these surveys, the DVL also provided AUV velocity over ground, allowing calculation of earth-referenced ocean current velocity. A corrective scaling factor for the water layer current velocity was calculated using established calibration methods [*Joyce*, 1989; *Pollard and Read*, 1989] and was verified by comparison of earth-referenced current velocities derived from coincident AUV and moored Acoustic Doppler Current Profiler (ADCP) data. Earth-referenced current velocity within the layer 5 to 20 m was averaged across the apex of two sequential sawtooth profiles. The resulting unevenly spaced velocity vectors (spacing dependent on water depth) were averaged into evenly spaced bins along the survey track. Errors in the velocity data presented are ~2 cm s^{-1}.

2.2.2. Moorings

[11] Data from oceanographic moorings were examined for cases in which slicks were observed directly over the mooring sites. Mooring locations are presented with the related SAR images in section 3. Two of the moorings were in shallow (~20 m) waters near the northern coast of Monterey Bay. The first is from the Partnership for Interdisciplinary Studies of the Coastal Ocean (PISCO) physical oceanography program, which monitored water column temperature and currents at Terrace Point (TPT1) [*Drake et al.*, 2005; *Woodson et al.*, 2007, 2009] (http://www.piscoweb.org/data). The second shallow water mooring was an autonomous vertical profiler [*Ryan et al.*, 2008b] deployed by MBARI near TPT1 for a 1 month process study. The profiler obtained hourly profiles between 4 m and near bottom (16 m) using Sea-Bird FastCAT CTD. The third mooring (M0), located in the northern bay on the 70 m

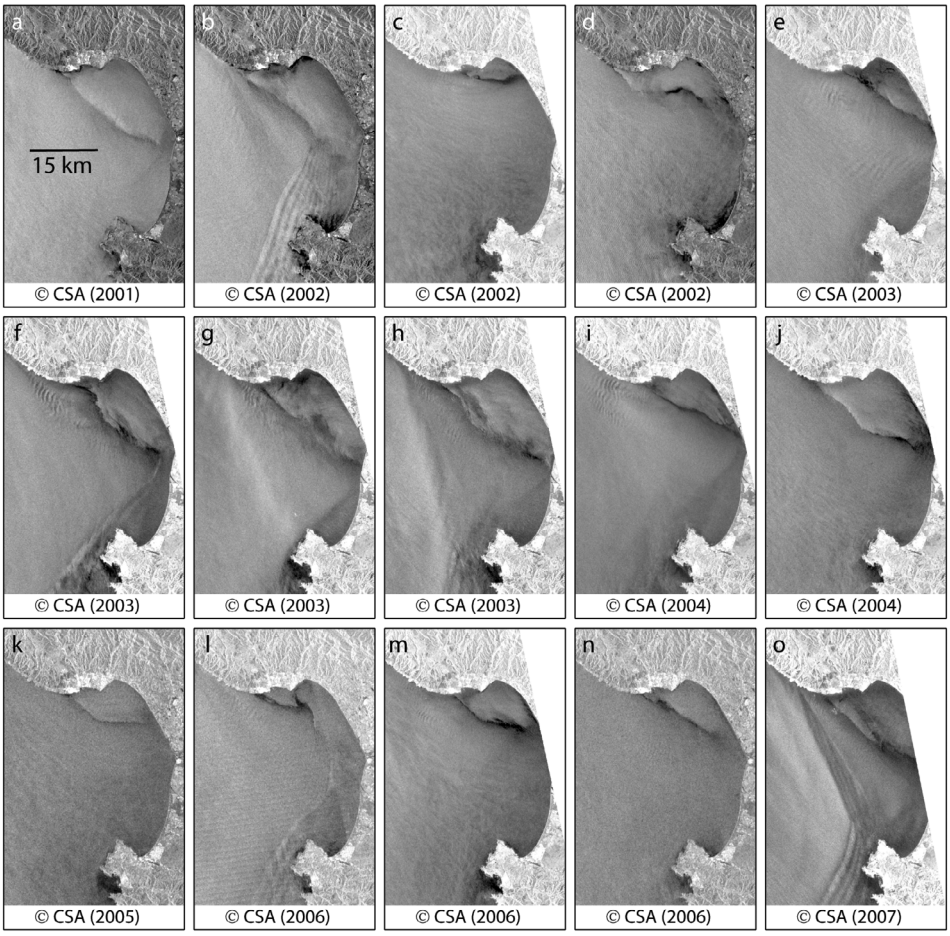

Figure 4. Examples of the recurrent pattern of slicks (narrow dark bands) across the northern Monterey Bay upwelling shadow.

isobath, provided data from a Sea-Bird Electronics SBE 37 MicroCAT conductivity, temperature, depth (CTD) sensor at 1 m depth.

2.2.3. Wind Data

[12] Wind data from two locations were used in this study: Long Marine Laboratory (LML) along the northern Monterey Bay coast, and mooring M1 at the mouth of the bay (locations are presented with results). At both locations, wind speed and direction were measured with a RM Young 5103 Wind Monitor for the same period as the SAR time series. Vector wind components were computed and averaged to hourly resolution. The first purpose of wind data analysis was evaluation of SAR imaging conditions. Because strong winds (>10 m s^{-1}) can mask slick detection in SAR [*Holt*, 2004], we analyzed wind speed data from M1 to evaluate potential masking effects within the analysis image set. Wind speeds for the hour concurrent with each SAR image acquisition were compared for (1) the full image set and (2) the subset in which slicks were detected. The second purpose of wind data analysis was to examine wind forcing relevant to slick development. Key regional wind forcing parameters include the direction and strength of alongshore winds. To determine if slicks were consistently associated with a single pattern of regional wind forcing, we computed average alongshore wind speed at M1 during the day preceding each slick detection by SAR. Key local wind forcing occurs by the diurnal sea breeze over northern Monterey Bay, which greatly affects MBUS along-coast transport [*Woodson et al.*, 2007, 2009]. To describe seasonal variation in the strength of the diurnal sea breeze, we computed the average diurnal cycle of alongshore winds at LML for each season, using 1998–2008 data. To describe the response of slick fronts to diurnal wind forcing, we identified cases in which a SAR image observed a slick directly over mooring TPT1, and we examined water column variation at TPT1 relative to alongshore winds.

3. Results

3.1. Slick Attributes

[13] The recurrent slick structures were introduced briefly in section 2 (Figures 2e and 2g). More representative examples illustrate (1) consistency in northwest-southeast orientation of the slicks' major axis across northern Monterey Bay and (2) variability in location, linearity, spatial dimensions, intensity, and cooccurrence with other physical signals (Figure 4). Measured slick attributes are summarized in Figure 5. Slicks ranged from 3.1 to 41.0 km in length

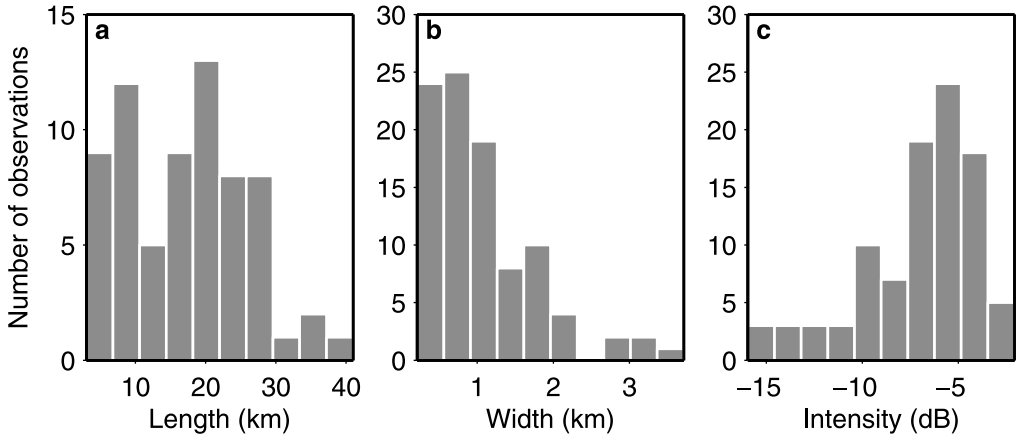

Figure 5. Histograms of slick length, width, and intensity (section 2.1.1).

(median 17.5 km) and 0.2 to 3.7 km in width (median 0.8 km). Their intensity (trough depth) ranged between −2.1 and −16.0 dB (median −6.3 dB). SAR sampling of slicks was not biased toward low wind speeds. Nearly the same percentage (18% of all analysis images and 15% of the subset containing slicks) coincided with wind speeds exceeding 10 m s^{-1}. Further, the averages of wind speeds exceeding 10 m s^{-1} were nearly equal in the slick subset (11.3 m s^{-1}) as in the full analysis set (11.7 m s^{-1}). Slicks coincided with regional wind forcing ranging from strong upwelling, to extremely weak winds, to strong downwelling.

3.2. Oceanographic Relationships

3.2.1. Sea Surface Temperature

[14] Limited sampling by SAR (Figure 3) and limited visibility for satellite SST coverage constrained the number of instances in which SAR detection of slicks could be examined with near-concurrent SST. Four examples having the most complete SST coverage of the bay are presented (Figure 6). In each example, the trace of the slick is overlaid on the SST image. Although the time differences (Δt on the SST images) introduce uncertainties in the degree to which direct comparison is possible, the matches presented are the best possible. All cases showed the positive onshore SST gradients across the northern bay associated with upwelling/shadow dynamics. However, slicks were not simply colocated with the locally strongest SST gradients, which were observed both seaward (Figure 6a) and shoreward (Figure 6b) of slicks. Instead, they were consistently located near the outer periphery of the relatively warm MBUS waters. Slicks generally paralleled isotherms, and the degree and pattern of slick bending was similar to that of isotherms (allowing for changes in surface patterns between the times of image acquisition). In one case, the southern extent of the slick crossed isotherms (Figure 6a).

3.2.2. Ocean Currents

[15] Slicks were observed to coincide with a variety of surface flow patterns, and to extend contiguously across zones of very different velocity (Figure 7). For example, some slicks coincided with strong seaward flow toward their northern end, and weak to near-zero flow toward their southern end (Figures 7a, 7b, and 7d). Some cases indicated uniform flow patterns across slicks (Figure 7a, northernmost portion of slick), while others indicated significant changes in flow patterns across the slick (Figure 7c, northernmost portion of slick). Significant spatial separation was observed between slicks and the shear front that is key to generating lateral gradients in heat advection along the front [*Graham and Largier*, 1997]. The southeastward jet of upwelling filament flow may be ~5–10 km seaward of the slicks (Figures 7a and 7b). This spatial separation is also evident in the location of the cold filament (Figure 6a) relative to the slick shown in Figure 7b. Influences of surface circulation patterns on slick locations and attributes were evident. For example, the slick that exhibited a large shoreward bend mirroring the intrusion of cold water (Figure 6a) also exhibited partial shoreward displacement and associated patchiness. The surface circulation shows that the shoreward displacement of the slick and isotherms were occurring along the eastern side of a cyclonic eddy in the northern bay (Figure 7b). This cyclonic eddy was part of a dipole, with an anticyclonic eddy on the seaward side of the southeastward flowing jet between them.

[16] Because horizontal shear can influence surface roughness patterns [*Lyzenga et al.*, 2004], we examined high-resolution sections of shallow layer velocity across the only two slicks for which near-concurrent AUV observations were available (Figure 8). In examining velocity in the layer between 5 and 20 m (section 2.2.1), it is important to acknowledge that water velocity above this layer may differ from that of the layer. However, we consider that the presence of strong shear directly underlying slicks should be evident in 5–20 m layer velocity. In the first case, velocity was uniform and shear was weak across the slick ±2 km (Figure 8a). In the second case, both velocity and shear were very weak across the slick (Figure 8b). Although there was a bay-wide shear associated with opposing meridional flow on either side of the low-velocity slick zone, shear was negligible in coincidence with the slick itself.

3.2.3. Water Column Relationships

[17] In situ observations illustrate a variety of complex processes occurring in the water column beneath slicks.

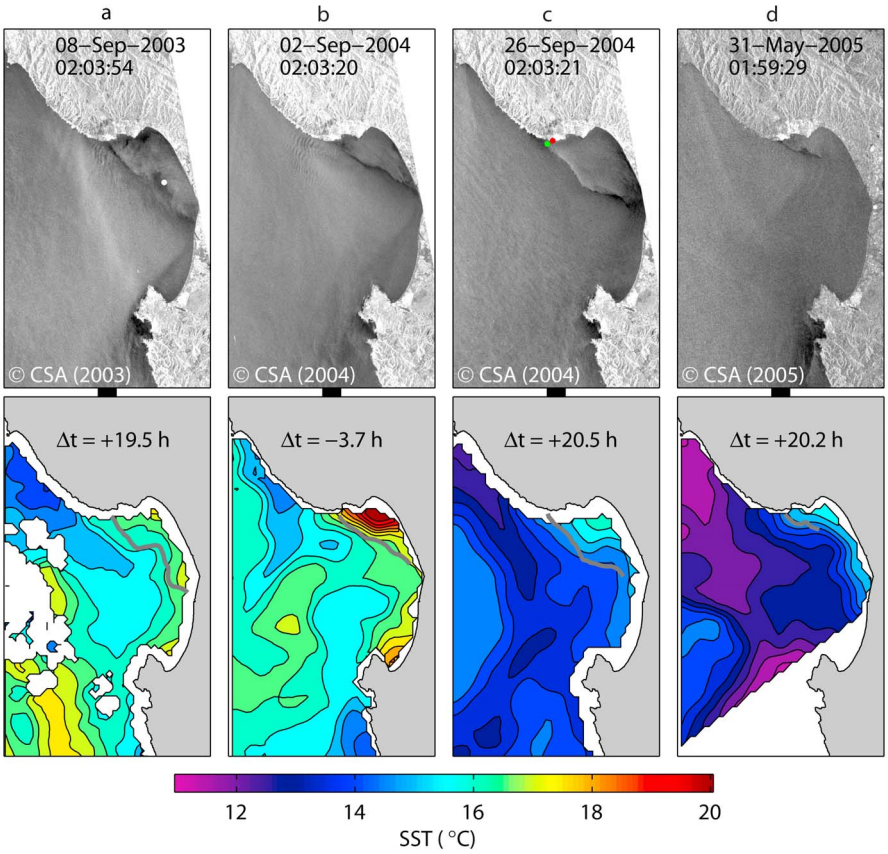

Figure 6. Examples of near-concurrent SAR images of slicks and AVHRR images of SST. SAR image acquisition times and dates are in UTC, and the time difference between the SST and SAR images is noted on each SST image. The trace of the shoreward edge of each slick is overlaid in the SST image (gray line). In the SAR image of Figure 6a the white circle shows the location of an autonomous vertical profiler mooring at which intense thin layers of phytoplankton were observed (section 3.2.3) [*Ryan et al.*, 2008b]. In the SAR image of Figure 6c the green circle shows the location of mooring TPT1 and the red circle shows the location of LML, from which water column and wind observations are later presented (Figure 9).

Physical-biological interactions were observed in the upwelling filament front associated with the slick shown in Figures 6a and 7b. Specifically, intense thin layers of phytoplankton were linked to patch thinning by vertical current shear at the location shown in Figure 6a [*Ryan et al.*, 2008b]. Another slick was observed directly overlying PISCO mooring TPT1 (green circle in Figure 6c). At the time of this SAR image acquisition, temperature at 5 m depth was rapidly decreasing following a period of strong onshore wind forcing (Figure 9). After the winds relaxed on 9/26, temperature increased rapidly. This pattern of wind forcing and thermal response was similarly evident in the preceding and following days and is consistent with the response of the warm, buoyant MBUS to diurnal wind forcing [*Woodson et al.*, 2009]. Specifically, warm MBUS waters retract into the bay following a period of onshore diurnal winds, and cooler waters from the north may pass across the mooring. Conversely, weakening and reversal of onshore winds permit buoyancy driven transport of warm MBUS waters northward along the coast, and warmer waters may pass across the mooring. There was also a consistent pattern of elevated acoustic backscatter in the shallow (3–5 m) frontal zone during the diurnal transition from warm to cool waters at the mooring site, that is, as warm MBUS waters retracted into Monterey Bay following onshore winds (Figure 9). Because elevated backscattering was not evident when the front moved northward over the mooring following relaxation of the diurnal onshore winds, it was evidently dependent upon wind forcing of the front. Elevated shallow acoustic backscattering has been observed in convergence zones of tidal fronts [*Farmer et al.*, 1995] and river plume fronts [*O'Donnell et al.*, 1998; *Trump and Marmorino*, 2003]. Alternative causes include injection of air bubbles and/or aggregation of zooplankton in the convergent front. There was only one other case study in which a slick was detected directly over TPT1. Although no ADCP acoustic backscatter data were available for this case, water column temperatures showed passage of the MBUS front past the mooring at the time of the SAR observation and a similar relationship between alongshore winds and frontal movement (not presented).

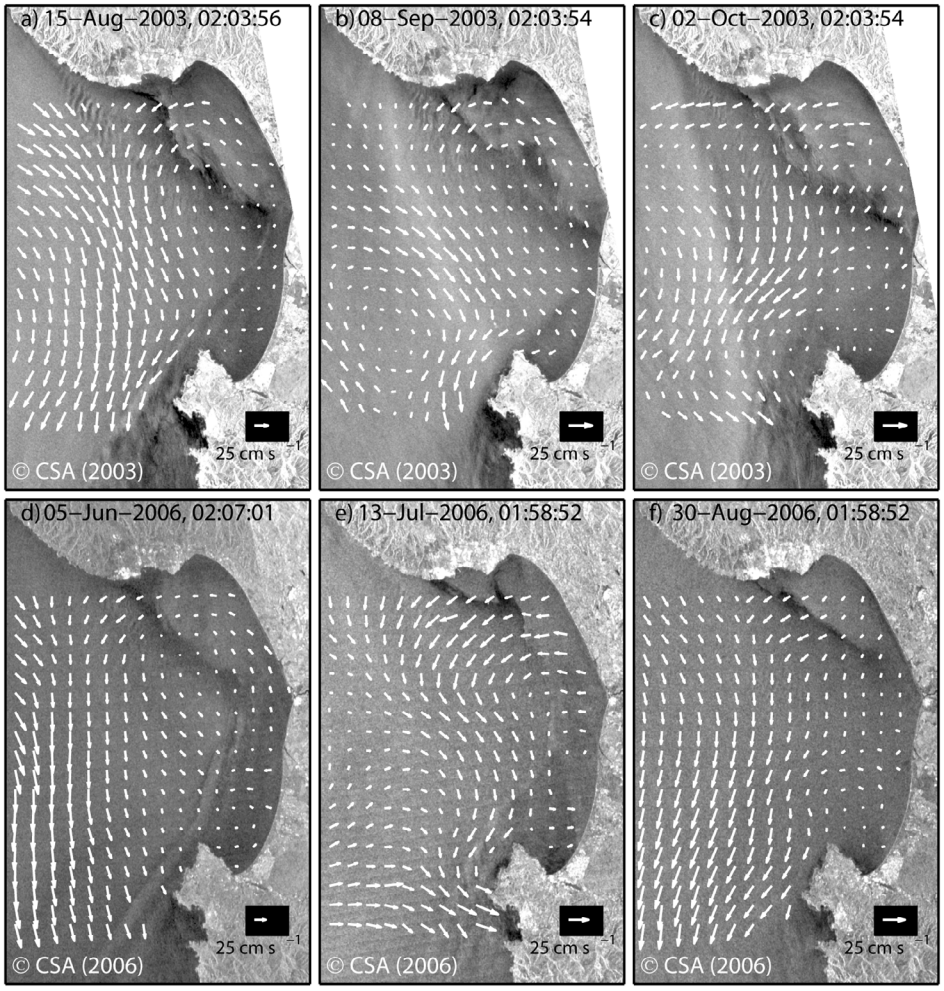

Figure 7. Examples of subtidal surface circulation patterns concurrent with SAR slick detection. Currents are 25 h averages ending at the hour of SAR image acquisition. Image acquisition times and dates are in UTC.

[18] Multiplatform in situ observations provided greater resolution of structure and processes in fronts underlying slicks. Two slicks concurrently extended across northern Monterey Bay on 4 September 2007 (Figure 10a). Data from a mooring within the western slick showed that the slick's presence coincided with approximately diurnal local oscillations in temperature and salinity (Figure 10c, 3–7 September). AUV surveys, beginning on the day of the SAR image (Figures 10a and 10c), showed warm waters occupying the upper water column of the northeast bay (Figure 11a). Warm waters extended further west toward the north, as would be hypothesized from the orientation of the slick in the SAR image (Figure 10a). These surveys also illustrate the complexity of the frontal zone. A low-salinity lens within the thermal front, at the southern limit of the survey (arrow in Figure 11a), identifies the basis for the temperature and salinity oscillations (Figure 10c). The oscillations are consistent with recurrent advection of the frontal zone temperature and salinity gradients across the mooring. Over the following 2 days, the low-salinity lens reduced in intensity and spread northward below the surface (arrows in Figures 11a–11c). These changes indicate that processes beneath the slick included lateral mixing, and subsurface cross-frontal transport of the low-salinity lens (northward; cf. Figures 10a and 11c).

[19] While temperature and salinity covaried at the southern mooring site that coincided with the western slick (Figure 10c), they varied inversely through a series of weaker oscillations at a northern mooring site that coincided with the eastern slick (Figure 10b). Thus, the two concurrent slicks were associated with different types of fronts. The later start of oscillations at the northern mooring site is consistent with the mooring's location just outside the eastern slick zone at the time of SAR image acquisition (Figure 10). The inverse relationship between temperature and salinity is evident in the northernmost east-west section of the AUV surveys that passed by this mooring site (Figure 11a).

[20] During early September 2005 a slick was observed twice in a similar configuration within a 3 day period, and an AUV surveyed beneath the slick (Figure 12). The slick was located near the isotherm outcropping of the warm upwelling shadow (Figure 12c). In this frontal zone, between ~36.87°N and 36.92°N, the coldest waters (<12°C) were shallowest (~11 m), the thermocline was strongest

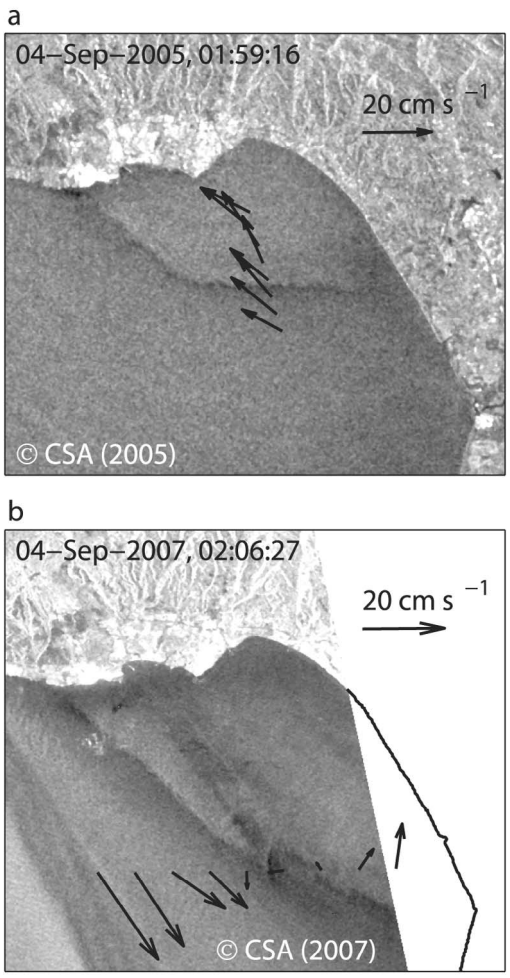

Figure 8. Shallow layer (5–20 m) earth-referenced velocity across slicks. (a) Velocity was measured between 1600 and 1900 UTC on 6 September 2005, ending 7 h before the SAR image acquisition. (b) Velocity was measured between 4 September 2134 and 5 September 0200 UTC 2007, between 20 and 24 h after the SAR image acquisition. The 4.5 h of this velocity data acquisition were centered on a slack tide.

(up to 0.45°C m^{-1}), and isotherms had the steepest slopes (0.01). These physical patterns indicate a dynamic frontal zone in the region of the slick.

3.3. Seasonal Dependence

[21] Slicks were detected year-round, with approximately half or more of the images exhibiting this structure in each season (Figure 13a). Diurnal winds, which are a primary forcing of the MBUS movement and frontal dynamics [*Woodson et al.*, 2007, 2009], are also an active influence year-round (Figure 13b). The 5 year AVHRR climatology shows that in all seasons, the warmest average SST in Monterey Bay is in the northeastern bay (Figure 14). Average SST gradients across the northern bay are strongest in summer, when upwelling is strongest, and weakest in winter. During winter, upwelling is not sustained as it is during the spring and summer, but rather occurs in episodic events of variable intensity, interspersed with periods of downwelling or very weak wind forcing [*Breaker and Broenkow*, 1994; *Graham and Largier*, 1997]. SST gradients across the northern bay during spring and fall are intermediate between winter and summer and of similar magnitude, although SST is warmer by ~3°C throughout the region during fall. Although seasonal variability is pronounced, all seasons exhibit the northwest-southeast orientation of isotherms marking the outer periphery of the MBUS.

4. Discussion

[22] The influences of retention and local surface heating in the MBUS were recognized in early oceanographic studies of Monterey Bay [*Bigelow and Leslie*, 1930]. Many studies since then have described physical, chemical and biological distinctions of MBUS waters [*Broenkow and Smethie*, 1978; *Graham et al.*, 1992; *Graham*, 1993; *Breaker and Broenkow*, 1994; *Rosenfeld et al.*, 1994; *Graham and Largier*, 1997; *Ryan et al.*, 2008a]. The first studies to describe northern Monterey Bay as an "upwelling shadow" noted that the strong temporal persistence of a feature having such a small spatial scale was somewhat unexpected [*Graham et al.*, 1992; *Graham*, 1993], yet such persistent small-scale features were apparently ubiquitous in coastal upwelling systems and likely to be extremely important to ecosystem structure and function [*Graham and Largier*, 1997]. The small scales of the MBUS and its dynamic responses to variation in wind forcing [e.g., *Woodson et al.*, 2007, 2009; *Ryan et al.*, 2009] make studies of its structure and function quite challenging. Yet more challenging is observing the structure and function of the seaward front of the MBUS. The development of enhanced zooplankton populations, including large gelatinous zooplankton, and enhanced tropic activity are characteristic of this front [*Graham et al.*, 1992; *Graham*, 1993]. Further, phytoplankton ecology studies have shown that the structure and dynamics of this front can result in enhanced growth, aggregation, and fine-scale layering of dense phytoplankton populations, including harmful algal bloom (HAB) species [*Ryan et al.*, 2008b, 2009, 2010a; *Jessup et al.*, 2009]. To emphasize the small scales that must be resolved in order to understand frontal ecology, we present an example of localized biological enhancement observed at two different spatial and spectral resolutions. A MODIS Aqua ocean color image, at relatively high resolution for satellite remote sensing (250 m), shows a green band oriented northwest-southeast across the northern bay, adjacent to waters more blue in color (label A in Figure 15a). Concurrent SST (not presented) shows that the blue waters were a cold upwelling filament flowing into and across the bay, and that the green band was located along the frontal zone between the upwelling filament and the MBUS. Inshore of this green band was an area of brownish surface color (label B in Figure 15a). An image from high-resolution airborne remote sensing on the same day (Figure 15b) shows that the MBUS frontal boundary had the highest green color enhancement in the bay, occurring at patch scales smaller than the satellite sensor could detect. Although near-concurrent SAR images were unavailable for this example of frontal biological structure, the location, spatial orientation and scale of the frontal enhancement are consistent with the characteristic

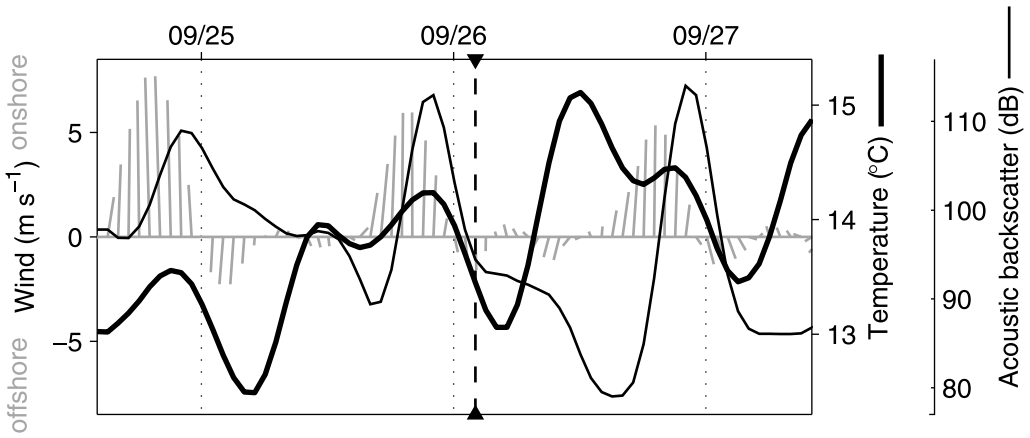

Figure 9. Time series of winds at LML and water column data at TPT1 (locations in Figure 6c) from a period during which a slick was detected directly overlying the TPT1 mooring. Onshore and offshore wind directions are indicated. TPT1 data are temperatures at 5 m and average acoustic backscatter in the layer 3–5 m. Time and date reference are in UTC; peak onshore winds are typically during midafternoon local time.

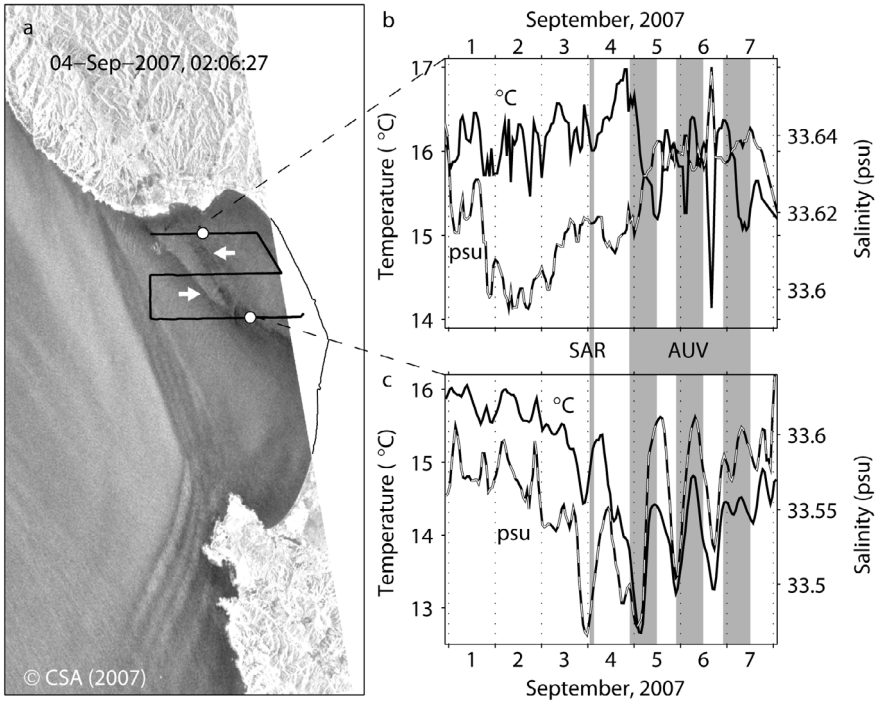

Figure 10. Remote and in situ observations of a slick and underlying front. (a) SAR image showing two slicks (white arrows) across northern Monterey Bay on 4 September 2007. The white circles show the locations of two moorings from which observations are presented in Figures 10b and 10c. The black line shows the surface track followed by a series of AUV surveys through the complex frontal/slick zone (Figure 11). (b) Hourly near-surface (4 m) temperature and salinity from the mooring coincident with the eastern slick zone. (c) Hourly near-surface (1 m) temperature and salinity from a mooring near the branching point of the two slicks as observed on 4 September. The times of the SAR image and the series of AUV surveys are indicated by gray shading in Figures 10b and 10c. The other significant structure in the SAR image, a wave-like pattern across the mouth of the bay, offshore of the identified slicks, may be due to atmospheric dynamics and air-sea coupling; this feature is not examined in this study.

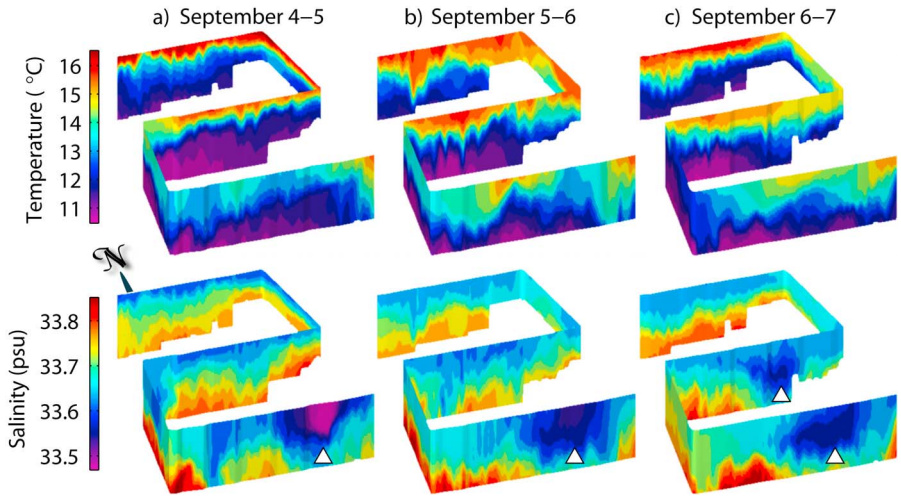

Figure 11. High-resolution vertical sections of temperature and salinity acquired along the AUV track shown in Figure 10a. The northward direction is indicated in the lower left. Survey times are shown in Figures 10b and 10c. Each section incorporated more than 600 profiles acquired in ~14 h. The depth range shown is 2–20 m. Arrows in the salinity sections identify an evolving low-salinity feature in the frontal zone (see text).

patterns of slicks detected by SAR along the MBUS front. Spectral resolution further shows that the brownish coloration observed inshore of the green band (label B in Figure 15a) had the strong near-infrared signal of a "red tide" bloom (Figure 15b) [e.g., *Ryan et al.*, 2009]. In the northern bay this reddish bloom was also connected with the dynamic ecological boundary of the MBUS front.

[23] While slicks along the seaward periphery of the MBUS have been noted descriptively in the literature [*Graham et al.*, 1992; *Graham*, 1993; *Graham and Largier*, 1997; *Woodson et al.*, 2007, 2009], no previous studies have acquired quantitative information about frontal slicks or variability in their relationships with thermal gradients. Further, ship-based studies of the front have focused on repeated transects across the MBUS at selected locations, precluding the acquisition of observations required to describe the synoptic patterns of slicks. The time series of SAR images examined in this study permitted the first systematic description of synoptic slick patterns of the MBUS. The high-resolution SAR data were essential to not only detect the narrow slicks, but also quantify their intensity, spatial patterns and scales, and year-round occurrence. The detection of slicks in all seasons may be somewhat surprising, considering that the original descriptions of the MBUS [*Graham et al.*, 1992; *Graham*, 1993] showed that onshore-offshore SST gradients along a cross-shadow transect were weak or absent during fall and winter. However, the single north-south transect, surveyed monthly for 15 months, was toward the outer bay and therefore did not sample the northeastern bay where sheltering and warming are strongest. Consistent with previous descriptions that illustrate episodic upwelling during winter [*Breaker and Broenkow*, 1994; *Graham and Largier*, 1997] and process studies examining the ecological significance of winter upwelling pulses [*Ryan et al.*, 2010b], the satellite SST climatology showed thermal distinction of the MBUS in winter. Stronger distinction in the means during other seasons is consistent with their more sustained upwelling.

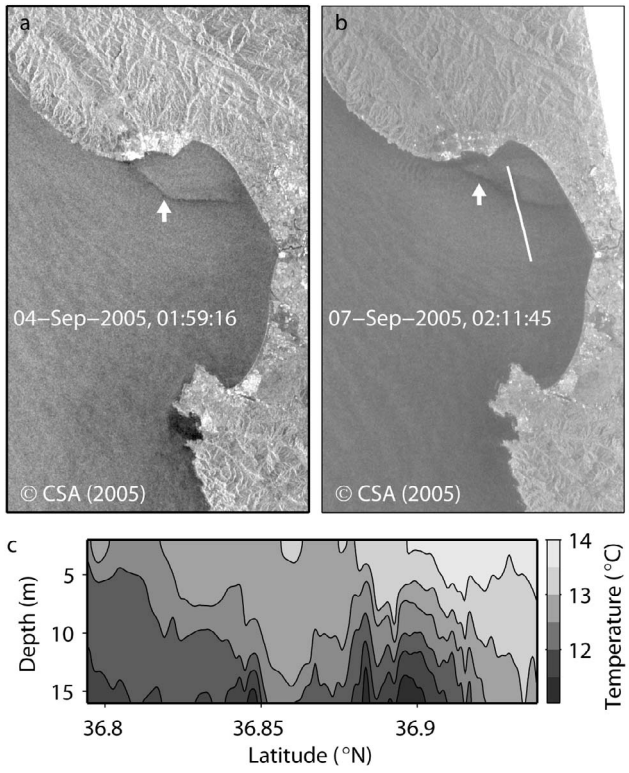

Figure 12. Remote and in situ observations of a slick and underlying front. (a, b) SAR images show a slick (arrows) across northern Monterey Bay on 4 and 7 September 2005. The white line in Figure 12b shows the surface track of the (c) temperature section, acquired by an AUV making 120 vertical profiles along the transect between 1600 and 1900 UTC on 6 September 2005, ending 7 h before the SAR image in Figure 12b.

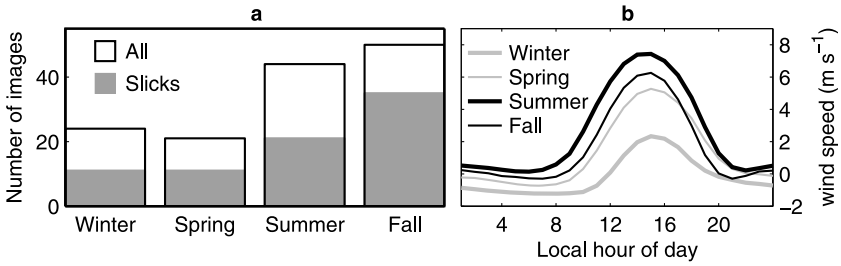

Figure 13. Seasonal descriptions. (a) Histograms of the seasonal counts of all SAR images examined, and the subset in which slicks were detected. (b) Seasonally averaged diurnal cycles of alongshore winds measured at LML (location in Figure 6c) between January 1998 and December 2008.

[24] A challenge in the interpretation ocean SAR imagery is the difficulty of distinguishing signals of oceanic, atmospheric and air-sea coupling processes. Oceanic and air-sea coupling processes may be detected in SAR due to (1) accumulation of surfactants that suppress short waves, (2) short wave-current interactions along convergence or shear zones, and (3) changes in atmospheric boundary layer stability across sharp SST gradients that influence small-scale patterns of air-sea frictional stress [*Holt*, 2004]. By its nature, the outer upwelling shadow is a strong shear zone [*Graham and Largier*, 1997], and studies have shown mesoscale air-sea coupling in the California Current System [*Chelton et al.*, 2007]. However, our study does not support either of these mechanisms as the direct cause of the slicks observed by SAR across the outer MBUS periphery.

[25] Shear is not indicated as the direct forcing of slicks because (1) synoptic high-resolution velocity sections showed no correspondence between slicks and locally enhanced shear and (2) near-concurrent SST and HF radar surface currents showed 5–10 km spatial separations between slicks and the shear front of the upwelling jet extending across the mouth of the bay. Such spatial separation may be due to strong lateral mixing between the upwelling jet and the upwelling shadow, which would locally reduce thermal gradients and preclude accumulation of surfactants in elongated bands. Airborne remote sensing of high spatial and temporal resolution has been used to document the strong lateral mixing that can occur in this zone as the inshore edge of an upwelling filament mixes with the upwelling shadow waters [*Ryan et al.*, 2009]. While shear is not indicated as directly forcing the slicks, it is certainly a key indirect forcing through heat advection and lateral mixing. These shear-driven processes interact with local heating and resultant buoyancy of northern bay waters to define the MBUS seaward periphery.

[26] Air-sea coupling is not indicated as the direct forcing because (1) slicks coincided with both equatorward and poleward wind forcing, showing that they are not constrained to a particular wind stress pattern and (2) the narrow cross-slick dimensions (median 0.8 km) and their curvature over small spatial scales, similar to SST isotherms, indicate oceanographic processes underlying their formation. Wind stress gradients develop in an orientation similar to the slicks during upwelling favorable (equatorward) wind forcing, with a positive wind stress gradient offshore [*Ramp et al.*, 2009], and this forcing may create divergence inshore of the wind jet. However, this process would not result in a narrow slick and could only disperse surfactants that are observed to aggregate at the MBUS front [*Graham et al.*, 1992; *Graham and Largier*, 1997; *Woodson et al.*, 2007]. Although convergence has not been directly measured across the MBUS front, the conditions that accompany the slicks (aggregation of buoyant macroalgae and foam) consistently indicate convergence. The accumulation of phytoplankton in convergent fronts, as suggested by Figure 15b, is also possible if the phytoplankton can swim toward the surface against the downwelling in the convergence. The importance of this process in shaping the distributions of dinoflagellate blooms in Monterey Bay is indicated by remote sensing and in situ observations [*Ryan et al.*, 2005a, 2008a, 2009, 2010a].

[27] Our integration of the SAR time series with multidisciplinary data from remote and in situ sensing permitted

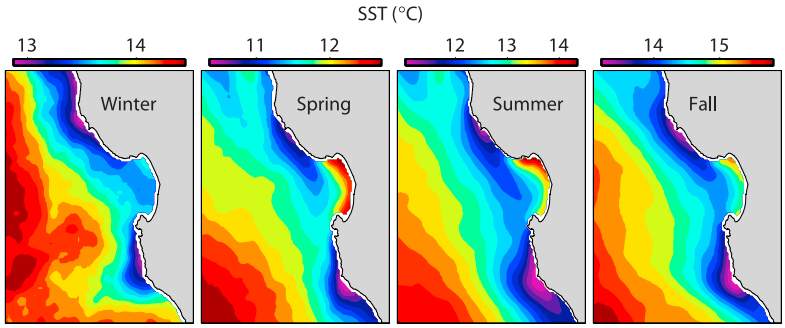

Figure 14. Seasonal SST climatology computed from 2004 to 2008 AVHRR data (section 2.1.2). To emphasize distinction of the MBUS in each season, color scaling of each seasonal mean is constrained to its SST range.

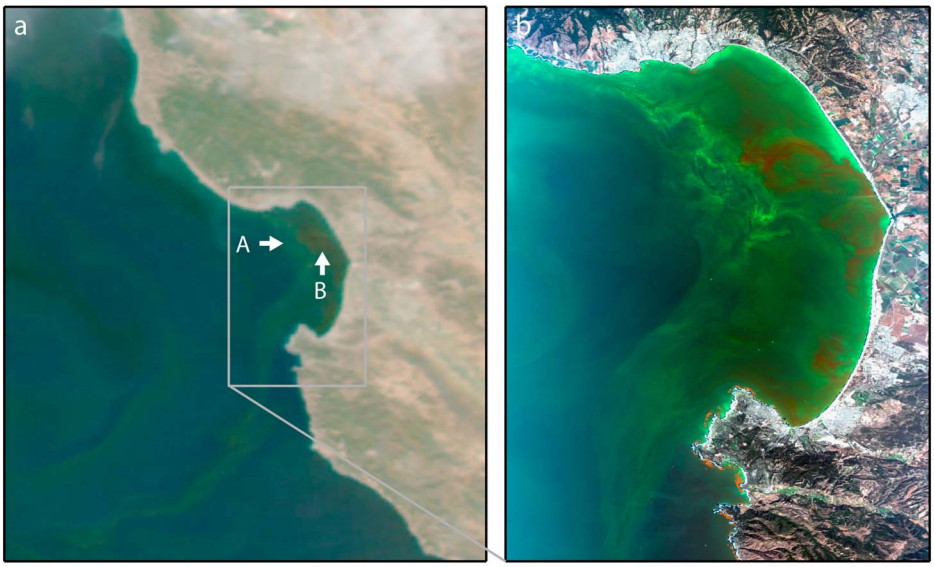

Figure 15. Ocean color observations illustrating biological structure of a front oriented across the outer MBUS, similar to the recurrent pattern of slicks detected by SAR (Figure 4). Both images are from 12 October 2004. (a) The MODIS true color image from 2150 UTC was produced with the SeaDAS software using the 469 nm (blue), 555 nm (green), and 645 nm (red) bands, having spatial resolutions of 500, 500, and 250 m, respectively. (b) The 34 m resolution MODIS Airborne Simulator image from 1930 GMT was produced with the ENVI software using the 462 nm (blue), 549 nm (green), and 704 nm (near-infrared) bands, at sensor radiance. The MAS 704 nm band is used to draw out the signal of "red tide" blooms, which appear reddish in this image. MODIS and MAS image processing methods are documented [*Ryan et al.*, 2009].

examination of the nature and environmental relationships of slicks. Slicks were not simply colocated with the strongest SST gradients, but rather were consistently located along the outer periphery of the buoyant MBUS warm lens, where convergence and subduction of cold waters occur [*Graham and Largier*, 1997; *Woodson et al.*, 2009]. As summarized in the introduction, convergent fronts have consequences for ecosystem structure and function that span life-form scales ranging from the microscopic to the largest marine mammals. High-resolution observations revealed ecologically important frontal zone processes at slicks. The most detailed in situ case study showed a low-salinity lens at a front in which lateral mixing and interleaving of regional water types were occurring. A study of harmful algal bloom (HAB) ecology during this same period showed that the frontal zone beneath the slick hosted a toxigenic phytoplankton species, at the highest cell concentrations observed during a 1 month study (D. I. Greenfield et al., unpublished data, 2007). Frontal zone transport patterns would determine whether the transport of toxic phytoplankton intersects with shellfish beds, through which vectoring to marine life and humans may occur. Accumulation of phytoplankton in frontal zones (e.g., Figure 15b) can magnify harmful effects, such as efficient transfer of toxins into the food web. Accumulation of buoyant surfactants in convergence zone slicks also has implications for a recently discovered HAB mechanism that does not involve toxins. Seabird mass mortality events along the northeastern Pacific coast have been linked to external coating of the birds by foam that fouls the insulating function of their feathers, causing hypothermia [*Jessup et al.*, 2009]. The causative foam has been traced to high concentrations of organic surfactants from dinoflagellate blooms. Accumulated surfactants are whipped into foam via turbulent mixing, and seabirds may encounter the harmful foam along the seashore and at offshore fronts.

[28] The finding of recurrent patterns in nature is a key step toward advancing the understanding and prediction of ecosystem variability. Although the ecological significance of marine fronts is well established in the literature, the complex processes forcing marine ecology at the relatively small scales of fronts are quite challenging to resolve. SAR can identify the narrow zones in which convergence and associated biological activity may be particularly energetic, and multidisciplinary, multiscale observations are essential to addressing this challenging research.

[29] **Acknowledgments.** This research was supported by the David and Lucile Packard Foundation. We thank the Canadian Space Agency (CSA) and NASA for providing RADARSAT-1 images through cooperative agreement. The acquisition and processing of SAR images were made possible by the Alaska Satellite Facility (ASF) and the developers of ASF's MapReady software. All AVHRR SST images were provided through the NOAA CoastWatch program, and AVHRR data processing was supported by the Central and Northern California Ocean Observing System (CeNCOOS) program. HF radar data was supported by the State of California's Coastal Ocean Currents Monitoring Program (COCMP). We thank the MODIS Airborne Simulator (MAS) team for acquisition of the MAS image presented in Figure 15b. Thermistor string and ADCP data for slick case studies were provided by the Partnership for Interdisciplinary Studies of the Coastal Ocean (PISCO) program. The wind data for Long Marine Laboratory were provided by R. Franks of the University of California, Santa Cruz.

References

Acha, E. M., and G. J. Macchi (2000), Spawning of Brazilian menhaden, *Brevoortia aurea*, in the Rio de la Plata estuary off Argentina and Uruguay, *Fish. Bull.*, *98*, 227–235.

Anderson, D. M., B. A. Keafer, W. R. Geyer, R. P. Signell, and T. C. Loder (2005), Toxic Alexandrium blooms in the western Gulf of Maine: The plume advection hypothesis revisited, *Limnol. Oceanogr.*, *50*, 328–345, doi:10.4319/lo.2005.50.1.0328.

Apel, J. R. (2004), Oceanic internal waves and solitons, in *Synthetic Aperture Radar Marine User's Manual*, edited by C. R. Jackson and J. R. Apel, pp. 189–206, NOAA, Washington, D. C.

Bakun, A. (1973), Coastal upwelling indices, west coast of North America, 1946–71, *Spec. Sci. Rep. 671*, 103 pp., Natl. Mar. Fish. Serv., Seattle, Wash.

Belkin, I. M. (2002), New challenge: Ocean fronts, *J. Mar. Syst.*, *37*, 1–2, doi:10.1016/S0924-7963(02)00191-4.

Belkin, I. M., P. C. Cornillon, and K. Sherman (2009), Fronts in large marine ecosystems, *Prog. Oceanogr.*, *81*, 223–236, doi:10.1016/j.pocean.2009.04.015.

Bigelow, H. B., and M. Leslie (1930), Reconnaissance of the waters and plankton of Monterey Bay, July 1928, *Bull. Mus. Comp. Zool.*, *70*, 429–581.

Bost, C. A., C. Cotte, F. Bailleul, Y. Cherel, J. B. Charrassin, C. Guinet, D. G. Ainley, and H. Weimerskirch (2009), The importance of oceanographic fronts to marine birds and mammals of the southern oceans, *J. Mar. Syst.*, *78*, 363–376, doi:10.1016/j.jmarsys.2008.11.022.

Breaker, L. C., and W. W. Broenkow (1994), The circulation of Monterey Bay and related processes, *Oceanogr. Mar. Biol.*, *32*, 1–64.

Broenkow, W. W., and W. M. Smethie (1978), Surface circulation and replacement of water in Monterey Bay, *Estuarine Coastal Mar. Sci.*, *6*, 583–603, doi:10.1016/0302-3524(78)90033-6.

Carreto, J. I., N. Montoya, R. Akselman, M. O. Carignan, R. I. Silva, and D. A. Cucchi Colleoni (2008), Algal pigment patterns and phytoplankton assemblages in different water masses of the Rio de la Plata maritime front, *Cont. Shelf Res.*, *28*, 1589–1606, doi:10.1016/j.csr.2007.02.012.

Castelao, R. M., T. P. Mavor, J. A. Barth, and L. C. Breaker (2006), Sea surface temperature fronts in the California Current System from geostationary satellite observations, *J. Geophys. Res.*, *111*, C09026, doi:10.1029/2006JC003541.

Chelton, D. B., M. G. Schlax, and R. M. Samelson (2007), Summertime coupling between sea surface temperature and wind stress in the California Current System, *J. Phys. Oceanogr.*, *37*, 495–517, doi:10.1175/JPO3025.1.

DiGiacomo, P. M., W. M. Hamner, P. P. Hamner, and R. M. A. Caldeira (2002), Phalaropes feeding at a coastal front in Santa Monica Bay, California, *J. Mar. Syst.*, *37*, 199–212, doi:10.1016/S0924-7963(02)00202-6.

Drake, P. T., M. A. McManus, and C. D. Storlazzi (2005), Local wind forcing of the Monterey Bay area inner shelf, *Cont. Shelf Res.*, *25*, 397–417, doi:10.1016/j.csr.2004.10.006.

Farmer, D. M., E. A. D'Asaro, M. V. Trevorrow, and G. T. Dairiki (1995), Three-dimensional structure in a tidal convergence front, *Cont. Shelf Res.*, *15*, 1649–1673, doi:10.1016/0278-4343(94)00084-Z.

Flament, P., L. Armi, and L. Washburn (1985), The evolving structure of an upwelling filament, *J. Geophys. Res.*, *90*, 11,765–11,778, doi:10.1029/JC090iC06p11765.

Franks, P. J. S. (1995), Thin layers of phytoplankton: A model of formation by near-inertial wave shear, *Deep Sea Res. Part I*, *42*, 75–83, doi:10.1016/0967-0637(94)00028-Q.

Govoni, J. J., B. W. Stender, and O. Pashuk (2000), Distribution of larval swordfish, *Xiphias gladius*, and probable spawning off the southeastern United States, *Fish. Bull.*, *98*, 64–74.

Graham, W. M. (1993), Spatio-temporal scale assessment of an 'upwelling shadow' in northern Monterey Bay, California, *Estuaries*, *16*, 83–91, doi:10.2307/1352766.

Graham, W. M., and J. L. Largier (1997), Upwelling shadows as nearshore retention sites: The example of northern Monterey Bay, *Cont. Shelf Res.*, *17*, 509–532, doi:10.1016/S0278-4343(96)00045-3.

Graham, W. M., J. G. Field, and D. C. Potts (1992), Persistent 'upwelling shadows' and their influence on zooplankton distributions, *Mar. Biol. Berlin*, *114*, 561–570, doi:10.1007/BF00357253.

Haney, J. C., and P. A. McGillivary (1985a), Midshelf fronts in the South Atlantic Bight and their influence on seabird distribution and seasonal abundance, *Biol. Oceanogr.*, *3*, 401–430.

Haney, J. C., and P. A. McGillivary (1985b), Aggregations of Cory's shearwaters (*Calonectris diomedea*) at Gulf Stream fronts, *Wilson Bull.*, *97*, 191–200.

Hollemans, P. (2005), CoastWatch software library and utilities user's guide, version 3.2.1, report, U.S. Dept. of Commerce, NOAA, Natl. Environ. Satell. Data and Inf. Serv., Washington, D. C. (Available at http://coralreefwatch.noaa.gov/satellite/software/cwf_3_2_1/cwf_ug_3_2_1.pdf.)

Holt, B. (2004), SAR imaging of the ocean surface, in *Synthetic Aperture Radar Marine User's Manual*, edited by C. R. Jackson and J. R. Apel, pp. 25–80, NOAA, Washington, D. C.

Janowitz, G. S., and D. Kamykowski (2006), Modeled *Karenia brevis* accumulation in the vicinity of a coastal nutrient front, *Mar. Ecol. Prog. Ser.*, *314*, 49–59, doi:10.3354/meps314049.

Jessup, D. A., M. A. Miller, J. P. Ryan, H. M. Nevins, H. A. Kerkering, A. Mekebri, D. B. Crane, T. A. Johnson, and R. M. Kudela (2009), Mass stranding of marine birds caused by a surfactant-producing red tide, *PLoS ONE*, *4*(2), E4550, doi:10.1371/journal.pone.0004550.

Joyce, T. M. (1989), On in situ calibration of shipboard ADCPs, *J. Atmos. Oceanic Technol.*, *6*, 169–172, doi:10.1175/1520-0426(1989)006<0169:OISOSA>2.0.CO;2.

Kudela, R. M., J. P. Ryan, M. D. Blakely, J. Q. Lane, and T. D. Peterson (2008), Linking the physiology and ecology of *Cochlodinium* to better understand harmful algal bloom events: A comparative approach, *Harmful Algae*, *7*, 278–292, doi:10.1016/j.hal.2007.12.016.

Lough, R. G., and J. P. Manning (2001), Tidal-front entrainment and retention of fish larvae on the southern flank of Georges Bank, *Deep Sea Res. Part II*, *48*, 631–644, doi:10.1016/S0967-0645(00)00130-2.

Lyzenga, D. R., G. O. Marmorino, and J. A. Johannessen (2004), Ocean currents and current gradients, in *Synthetic Aperture Radar Marine User's Manual*, edited by C. R. Jackson and J. R. Apel, pp. 207–220, NOAA, Washington, D. C.

Marmorino, G., F. Askari, and R. Mied (2002), Observations of the creation and evolution of small-scale oceanic frontal cusps and slicks, *J. Mar. Syst.*, *37*, 17–29, doi:10.1016/S0924-7963(02)00193-8.

McLaren, I. A., P. Avendano, C. T. Taggart, and S. E. Lochmann (1998), Feeding by larval cod in different water-masses on Western Bank, Scotian Shelf, *Fish. Oceanogr.*, *6*, 250–265, doi:10.1046/j.1365-2419.1998.00044.x.

McManus, M. A., R. M. Kudela, M. W. Silver, G. F. Steward, P. L. Donaghay, and J. M. Sullivan (2008), Cryptic blooms: Are thin layers the missing connection?, *Estuaries Coasts*, *31*, 396–401, doi:10.1007/s12237-007-9025-4.

Moore, J. K., and M. R. Abbott (2002), Surface chlorophyll concentrations in relation to the Antarctic Polar Front: Seasonal and spatial patterns from satellite observations, *J. Mar. Syst.*, *37*, 69–86, doi:10.1016/S0924-7963(02)00196-3.

Morgan, C. A., A. De Robertis, and R. W. Zabel (2005), Columbia River plume fronts. Part I. Hydrography, zooplankton distribution, and community composition, *Mar. Ecol. Prog. Ser.*, *299*, 19–31, doi:10.3354/meps299019.

O'Donnell, J., G. O. Marmorino, and C. L. Trump (1998), Convergence and downwelling at a river plume front, *J. Phys. Oceanogr.*, *28*, 1481–1495, doi:10.1175/1520-0485(1998)028<1481:CADAAR>2.0.CO;2.

Paduan, J. D., and H. C. Graber (1997), Introduction to high frequency radar: Reality and myth, *Oceanography*, *10*, 36–39.

Paduan, J. D., and L. K. Rosenfeld (1996), Remotely sensed surface currents in Monterey Bay from shore-based HF radar (CODAR), *J. Geophys. Res.*, *101*, 20,669–20,686, doi:10.1029/96JC01663.

Paduan, J. D., K. C. Kim, M. S. Cook, and F. P. Chavez (2006), Calibration and validation of direction-finding high frequency radar ocean surface current observations, *IEEE J. Oceanic Eng.*, *31*, 862–875, doi:10.1109/JOE.2006.886195.

Pennington, J. T., and F. P. Chavez (2000), Seasonal fluctuations of temperature, salinity, nitrate, chlorophyll and primary production at station H3/M1 over 1989–1996 in Monterey Bay, California, *Deep Sea Res, Part II*, *47*, 947–973, doi:10.1016/S0967-0645(99)00132-0.

Pingree, R. D., G. R. Forster, and G. K. Morrison (1974), Turbulent convergent tidal fronts, *J. Mar. Biol. Assoc. U. K.*, *54*, 469–479, doi:10.1017/S0025315400058653.

Pingree, R. D., P. R. Pugh, P. M. Holligan, and G. R. Forster (1975), Summer phytoplankton blooms and red tides along tidal fronts in the approaches to the English Channel, *Nature*, *258*, 672–677, doi:10.1038/258672a0.

Pitcher, G. C., A. J. Boyd, D. A. Horstman, and B. A. Mitchell-Innes (1998), Subsurface dinoflagellate populations, frontal blooms and the formation of red tide in the southern Benguela upwelling system, *Mar. Ecol. Prog. Ser.*, *172*, 253–264, doi:10.3354/meps172253.

Pollard, R., and J. Read (1989), A method for ship-mounted acoustic Doppler profilers and the limitations of gyrocompasses, *J. Atmos. Oceanic Technol.*, *6*, 859–865, doi:10.1175/1520-0426(1989)006<0859:AMFCSA>2.0.CO;2.

Polovina, J. J., G. H. Balazs, E. A. Howell, D. M. Parker, M. P. Seki, and P. H. Dutton (2004), Forage and migration habitat of loggerhead (*Caretta caretta*) and olive ridley (*Lepidochelys olivacea*) sea turtles in the central

North Pacific Ocean, *Fish. Oceanogr.*, *13*, 36–51, doi:10.1046/j.1365-2419.2003.00270.x.

Ramp, S. R., J. D. Paduan, I. Shulman, J. Kindle, F. L. Bahr, and F. Chavez (2005), Observations of upwelling and relaxation events in the northern Monterey Bay during August 2000, *J. Geophys. Res.*, *110*, C07013, doi:10.1029/2004JC002538.

Ramp, S. R., et al. (2009), Preparing to predict: The second autonomous ocean sampling network (AOSN-II) experiment in Monterey Bay, *Deep Sea Res. Part II*, *56*, 68–86, doi:10.1016/j.dsr2.2008.08.013.

Rienecker, E. R., J. P. Ryan, R. Marin III, M. Blum, C. Dietz, and F. P. Chavez (2008), Synoptic mapping of the phytoplankton size distribution, with applications to the ecology of red tides and harmful algal blooms, *Limnol. Oceanogr. Methods*, *6*, 153–161.

Rosenfeld, L. K., F. B. Schwing, N. Garfield, and D. E. Tracy (1994), Bifurcated flow from an upwelling center: A cold water source for Monterey Bay, *Cont. Shelf Res.*, *14*, 931–964, doi:10.1016/0278-4343(94)90058-2.

Roughgarden, J., J. T. Pennington, D. Stoner, S. Alexander, and K. Miller (1991), Collisions of upwelling fronts with the intertidal zone: The cause of recruitment pulses in barnacle populations of central California, *Acta Oecol.*, *12*, 35–51.

Russell, R. W., N. M. Harrison, and G. L. Hunt (1999), Foraging at a front: Hydrography, zooplankton, and avian planktivory in the northern Bering Sea, *Mar. Ecol. Prog. Ser.*, *182*, 77–93, doi:10.3354/meps182077.

Ryan, J. P., and J. A. Yoder (1996), Long-term mean and event-related pigment distributions during the unstratified period in South Atlantic Bight outer margin and middle shelf waters, *Cont. Shelf Res.*, *16*, 1165–1183, doi:10.1016/0278-4343(95)00062-3.

Ryan, J. P., J. A. Yoder, and P. C. Cornillon (1999a), Enhanced chlorophyll at the shelfbreak of the Mid-Atlantic Bight and Georges Bank during the spring transition, *Limnol. Oceanogr.*, *44*, 1–11, doi:10.4319/lo.1999.44.1.0001.

Ryan, J. P., J. A. Yoder, P. C. Cornillon, and J. A. Barth (1999b), Chlorophyll enhancement and mixing associated with meanders of the shelfbreak front in the Mid-Atlantic Bight, *J. Geophys. Res.*, *104*, 23,479–23,493, doi:10.1029/1999JC900174.

Ryan, J. P., J. A. Yoder, and D. W. Townsend (2001), Influence of a Gulf Stream warm-core ring on water mass and chlorophyll distributions along the southern flank of Georges Bank, *Deep Sea Res. Part II*, *48*, 159–178, doi:10.1016/S0967-0645(00)00117-X.

Ryan, J. P., H. M. Dierssen, R. M. Kudela, C. A. Scholin, K. S. Johnson, J. M. Sullivan, A. M. Fischer, E. V. Rienecker, P. R. McEnaney, and F. P. Chavez (2005a), Coastal ocean physics and red tides, an example from Monterey Bay, California, *Oceanography*, *18*, 246–255.

Ryan, J. P., F. P. Chavez, and J. G. Bellingham (2005b), Physical-biological coupling in Monterey Bay, California: Topographic influences on phytoplankton ecology, *Mar. Ecol. Prog. Ser.*, *287*, 23–32, doi:10.3354/meps287023.

Ryan, J. P., J. F. R. Gower, S. A. King, W. P. Bissett, A. M. Fischer, R. M. Kudela, Z. Kolber, F. Mazzillo, E. V. Rienecker, and F. P. Chavez (2008a), A coastal ocean extreme bloom incubator, *Geophys. Res. Lett.*, *35*, L12602, doi:10.1029/2008GL034081.

Ryan, J. P., M. A. McManus, J. D. Paduan, and F. P. Chavez (2008b), Phytoplankton thin layers within coastal upwelling system fronts, *Mar. Ecol. Prog. Ser.*, *354*, 21–34, doi:10.3354/meps07222.

Ryan, J. P., A. M. Fischer, R. M. Kudela, J. F. R. Gower, S. A. King, R. Marin III, and F. P. Chavez (2009), Influences of upwelling and downwelling winds on red tide bloom dynamics in Monterey Bay, California, *Cont. Shelf Res.*, *29*, 785–795, doi:10.1016/j.csr.2008.11.006.

Ryan, J. P., M. A. McManus, and J. M. Sullivan (2010a), Interacting physical, chemical and biological forcing of phytoplankton thin-layer variability in Monterey Bay, California, *Cont. Shelf Res.*, *30*, 7–16, doi:10.1016/j.csr.2009.10.017.

Ryan, J. P., S. B. Johnson, A. Sherman, K. Rajan, F. Py, H. Thomas, J. B. J. Harvey, L. Bird, J. D. Paduan, and R. C. Vrijenhoek (2010b), Mobile autonomous process sampling within coastal ocean observing systems, *Limnol. Oceanogr. Methods*, *8*, 394–402, doi:10.4319/lom.2010.8.394.

Sabates, A., M. P. Olivar, J. Salat, I. Palomera, and F. Alemany (2007), Physical and biological processes controlling the distribution of fish larvae in the NW Mediterranean, *Prog. Oceanogr.*, *74*, 355–376, doi:10.1016/j.pocean.2007.04.017.

Schiariti, A., A. D. Berasategui, D. A. Giberto, R. A. Guerrero, E. M. Acha, and H. W. Mianzan (2006), Living in the front: *Neomysis americana* (Mysidacea) in the Rio de la Plata estuary, Argentina-Uruguay, *Mar. Biol. Berlin*, *149*, 483–489, doi:10.1007/s00227-006-0248-x.

Shanks, A. L., J. Largier, L. Brink, J. Brubaker, and R. Hooff (2000), Demonstration of the onshore transport of larval invertebrates by the shoreward movement of an upwelling front, *Limnol. Oceanogr.*, *45*, 230–236, doi:10.4319/lo.2000.45.1.0230.

Simpson, J. H., and R. D. Pingree (1978), Shallow sea fronts produced by tidal stirring, in *Oceanic Fronts in Coastal Processes*, edited by M. J. Bowman and W. E. Esiais, pp. 29–42, Springer, New York.

Skaröhamar, J., D. Slagstad, and A. Edvardsen (2007), Plankton distributions related to hydrography and circulation dynamics on a narrow continental shelf off Northern Norway, *Estuarine Coastal Shelf Sci.*, *75*, 381–392, doi:10.1016/j.ecss.2007.05.044.

Smayda, T. J. (2002), Turbulence, watermass stratification and harmful algal blooms: An alternative view and frontal zones as pelagic seed banks, *Harmful Algae*, *1*, 95–112, doi:10.1016/S1568-9883(02)00010-0.

Tester, P. A., and K. A. Steidinger (1997), *Gymnodinium breve* red tide blooms: Initiation, transport, and consequences of surface circulation, *Limnol. Oceanogr.*, *42*, 1039–1051, doi:10.4319/lo.1997.42.5_part_2.1039.

Tilburg, C. E., A. I. Dittel, and C. E. Epifanio (2009), High concentrations of blue crab (*Callinectes sapidus*) larvae along the offshore edge of a coastal current: Effects of convergent circulation, *Fish. Oceanogr.*, *18*, 135–146, doi:10.1111/j.1365-2419.2009.00502.x.

Trump, C. L., and G. O. Marmorino (2003), Mapping small-scale along-front structure using ADCP acoustic backscatter range-bin data, *Estuaries*, *26*, 878–884, doi:10.1007/BF02803346.

Uye, S.-I., T. Yamaoka, and T. Fujisawa (1992), Are tidal fronts good recruitment areas for herbivorous copepods?, *Fish. Oceanogr.*, *1*, 216–226, doi:10.1111/j.1365-2419.1992.tb00040.x.

Woehler, E. J., B. Raymond, and D. J. Watts (2006), Convergence or divergence: Where do short-tailed shearwaters forage in the Southern Ocean?, *Mar. Ecol. Prog. Ser.*, *324*, 261–270, doi:10.3354/meps324261.

Woodson, C. B., et al. (2007), Local diurnal upwelling driven by sea breezes in northern Monterey Bay, *Cont. Shelf Res.*, *27*, 2289–2302, doi:10.1016/j.csr.2007.05.014.

Woodson, C. B., L. Washburn, J. A. Barth, D. J. Hoover, A. R. Kirincich, M. A. McManus, J. P. Ryan, and J. Tyburczy (2009), Northern Monterey Bay upwelling shadow front: Observations of a coastally and surface-trapped buoyant plume, *J. Geophys. Res.*, *114*, C12013, doi:10.1029/2009JC005623.

Yoder, J. A., L. P. Atkinson, T. N. Lee, H. H. Kim, and C. R. McClain (1981), Role of Gulf Stream frontal eddies in forming phytoplankton patches on the outer southeastern shelf, *Limnol. Oceanogr.*, *26*, 1103–1110, doi:10.4319/lo.1981.26.6.1103.

A. M. Fischer, National Centre for Marine Conservation and Resource Sustainability, University of Tasmania, Locked Bag 1370, Launceston, TAS 7250, Australia.

R. M. Kudela and C. M. Ruhsam, Ocean Sciences Department, University of California, Santa Cruz, CA 95064, USA.

M. A. McManus, Department of Oceanography, University of Hawaii at Manoa, 1000 Pope Rd., Honolulu, HI 96822, USA.

J. S. Myers, University Affiliated Research Center, University of California, Santa Cruz, MS 244-15, Moffett Field, CA 94035, USA.

J. D. Paduan, Department of Oceanography, Naval Postgraduate School, 411 Dyer Rd., Monterey, CA 93943, USA.

J. Ryan and Y. Zhang, Monterey Bay Aquarium Research Institute, 7700 Sandholdt Rd., Moss Landing, CA 95062, USA. (ryjo@mbari.org)

C. B. Woodson, Environmental Fluid Mechanics Laboratory, Department of Civil and Environmental Engineering, Stanford University, Stanford, CA 95039, USA.